Alp-Erbay, E.; Figueroa-López, KJ.; Lagaron, JM.; Çaglak, E.; Torres-Giner, S. (2019). The impact of electrospun films of poly(epsilon-caprolactone) filled with nanostructured zeolite and silica microparticles on in vitro histamine formation by Staphylococcus aureus and Salmonella Paratyphi A. Food Packaging and Shelf Life. 22:1-13. https://doi.org/10.1016/j.fpsl.2019.100414

The impact of electrospun films of poly(ε-caprolactone) filled with nanostructured zeolite and silica microparticles on *in vitro* histamine formation by *Staphylococcus aureus* and *Salmonella* Paratyphi A

Esen Alp-Erbay [a], Kelly J. Figueroa-Lopez [b], José M. Lagaron [b], Emre Çağlak [c], Sergio Torres-Giner [b,*]

[a] Central Fisheries Research Institute (SUMAE), Food Technology Department, Vali Adil Yazar Ave. 14, Kaşüstü, Yomra, 61250 Trabzon, Turkey.

[b] Novel Materials and Nanotechnology Group, Institute of Agrochemistry and Food Technology (IATA), Spanish National Research Council (CSIC), Calle Catedrático Agustín Escardino Benlloch 7, 46980 Paterna, Spain.

[c] Recep Tayyip Erdoğan University, Faculty of Fisheries, Department of Processing Technology, Su Ürünleri Fakültesi Zihni Derin Yerleşkesi, 53100 Rize, Turkey.

* Corresponding author: storresginer@iata.csic.es; Tel.: +34-963-900-022

Abstract. This study originally reports the preparation and characterization of electrospun films based on poly(ε-caprolactone) (PCL) with high histamine-binding capacity. To this end, submicron PCL fibers filled with nanostructured zeolite or silica (SiO_2) microparticles in the 5–20 wt% range were first prepared by electrospinning. The resultant electrospun composite fiber mats were thereafter thermally post-treated at 55 °C to successfully develop contact-transparent films with reduced porosity and improved mechanical strength. The capacity of the developed composite films to entrap histamine was evaluated *in vitro* by the culture media method using *Staphylococcus aureus* (*S. aureus*) and *Salmonella* Paratyphi A (*S.* Paratyphi A) food-borne bacteria. Both electrospun zeolite- and SiO_2-containing PCL films exhibited high histamine-binding capacity, being more effective for *S. aureus.* The histamine entrapment performance was significantly higher for the PCL films filled with zeolite due to the enhanced porous structure and more optimal adsorption selectivity of this mineral. The here-developed electrospun composite films can be originally applied as novel active-scavenging packaging materials to entrap heat-stable histamine and other biogenic amines released from fish and fishery products.

Keywords: PCL; Zeolite; Silica; Histamine; Active packaging; Food preservation

1. Introduction

Amines are basic nitrogenous compounds in which one, two or three atoms of hydrogen in ammonia are replaced by alkyl or aryl groups. Amines are designated "biogenic" when they are produced by the action of living organisms through the decarboxylation process of amino acids (Shalaby, 1996). One of the most important biogenic amines occurring in fish and fishery products is histamine. High levels of histamine are usually formed during decomposition or spoilage process of fish, involving formation of free amino acids through proteolysis together with bacterial production and action of amino acid decarboxylases (Visciano, Schirone, Tofalo, & Suzzi, 2012). Fish of the families *Scombridae* and *Scomberesocideae*, which include mackerel, tunas, saury, bonito, seerfish, and butterfly kingfish, are commonly involved in incidents of histamine poisoning (Taylor & Eitenmiller, 1986). Non-scombroid fish such as sardine, pilchards, anchovies, herring and marlin, have also been implicated. (Taylor, Smith, & Calaby, 1985). These species of fish have the naturally occurring amino acid histidine in their flesh and some spoilage bacteria rich in the enzyme histidine decarboxylase can proliferate and produce histamine (Hungerford, 2010; Kimura, Konagaya, & Fujii, 2001; Kung et al., 2009; Laganà et al., 2015; López-Sabater, Rodríguez-Jerez, Roig-Sagués, & Teresa Mora-Ventura, 1994). Gram-positive (G+) histamine-producing bacteria typically belong to the *Staphylococcus* strain (Chang, Kung, Chen, Lin, & Tsai, 2008; Kuley & Özogul, 2011; Simon & Sanjeev, 2007; Zarei, Maktabi, & Ghorbanpour, 2012), which can be isolated from fresh fish and shrimp (Lakshmanan, Shakila, & Jeyasekaran, 2002), fermented foods such as wine, cheese and fish sauce (Satomi, 2016), salted fish (Hernández-Herrero, Roig-Sagués, Rodríguez-Jerez, & Mora-Ventura, 1999), and other fishery products (Gokdogan et al., 2012; Özogul, Kacar, & Hamed, 2015). *Salmonella* Gram-negative (G-) bacteria of *Enterobacteriaceae* family have also been reported to be a histamine producer strain (Georgnaras, Dykes, & Holy, 1995; Gokdogan et al., 2012; Kuley et al., 2017; Özogul et al., 2015).

Heat-stable histamine is mostly formed at excessive temperatures of storage for fresh fish and prolonged handling at ambient temperatures for processed products. Bacteria responsible from histamine formation are either contaminants of post-harvest fish or natural flora of fish tissue and intestines. The United States Food and Drug Administration (FDA) and European Community (EC)

55 established the permissible limit of histamine in edible fish at 50 mg/kg (USFDA-CFSAN, 2011) and
56 200 mg/kg (European Communities, 1991), respectively. Histamine poisoning can result from the
57 ingestion of food containing high levels of histamine (Stratton, Hutkins, & Taylor, 1991), which is
58 manifested by a wide variety of symptoms affecting the cutaneous system (*e.g.* rash, urticaria, edema,
59 and localized inflammation) (Taylor & Eitenmiller, 1986), gastrointestinal involvements (*e.g.* nausea,
60 vomiting, diarrhea, and abdominal cramps) (Murray, Hobbs, & Gilbert, 1982; Taylor & Eitenmiller,
61 1986), and other symptoms such as hypotension, headache, palpitation, tingling, flushing, etc.
62 (Gilbert, Hobbs, Murray, Cruickshank, & Young, 1980; Taylor et al., 1985). One of the major
63 challenges in preventing histamine poisoning is the difficulty in guessing histamine accumulation in
64 fish flesh based on their appearance (Lehane & Olley, 2000; Nei, 2014). Moreover, the removal of
65 histamine in fish flesh is difficult once it is produced since it is a heat-stable compound, even with
66 cooking and prolonged heating (Tapingkae et al., 2010). Traditionally, histamine is mainly prevented
67 by limiting microbial growth during storage using chilling and freezing. However, histamine cannot
68 be inactivated by freezing, chilling, cooking, and canning (Ahmed, 2019). Also, supplying a whole
69 cold chain is not frequently practical for small scale producers. Therefore, alternative control
70 techniques are required to prevent histamine formation or to reduce their levels once formed (Naila,
71 Flint, Fletcher, Bremer, & Meerdink, 2010).

72 In the last years, the electrospinning technology has received a great deal of attention as a technique
73 for the production of polymer-based nanofibers with bioactive properties with a particular emphasis
74 in the active and bioactive packaging field (Torres-Giner, Perez-Masia, & Lagaron, 2016). In this
75 regard, electrospun nanofibers can be applied as monolayers and coatings or interlayers in multilayers
76 to generate novel films with controlled release capacity of natural antimicrobial or antioxidant
77 substances (Alp-Erbay, Yeşilsu, & Türe, 2019; Quiles-Carrillo, Montanes, Lagaron, Balart, & Torres-
78 Giner, 2019; Torres-Giner, Martinez-Abad, & Lagaron, 2014). To this end, the electrospun polymer
79 mats can be subjected to annealing, a thermal post-treatment below the polymer's melting point (T_m),
80 to form continuous and homogeneous films by a process of nanofibers coalescence and rearrangement

(Cherpinski, Torres-Giner, Cabedo, & Lagaron, 2017; Lasprilla-Botero, Torres-Giner, Pardo-Figuerez, Álvarez-Láinez, & Lagaron, 2018; Melendez-Rodriguez et al., 2018).

The use of electrospun films opens up novel opportunities in intelligent packaging since they can be functionalized by the incorporation of organic substances, inorganic fillers, and metallic nanoparticles (MNPs) at room conditions (Torres-Giner et al., 2018). Poly(ε-caprolactone) (PCL) is biodegradable in nature and biocompatible due to the susceptibility of its aliphatic ester linkage to hydrolysis. Therefore, electrospinning of PCL solutions results in nanofiber mats of high interest in tissue engineering applications (Jin et al., 2013; Sridhar et al., 2014) but also in food preservation (Alp-Erbay, Dağtekin, Türe, Yeşilsu, & Torres-Giner, 2017) due to this biopolymer has been reported to be safe by the Food and Drug Administration (FDA) (Filipczak et al., 2005; Wang, Zhao, Turng, & Li, 2013). For active-scavenging systems, the PCL biopolymer is particularly suitable based on its intrinsically high permeability characteristics (Mohamed & Yusoh, 2015; Woodruff & Hutmacher, 2010). Microparticles of both zeolite aluminosilicate (Huwig, Freimund, Käppeli, & Dutler, 2001) and silica (SiO_2) (Showkat et al., 2007) have received a great deal of attention because of their high cation exchange capability and molecular sieving. The nanostructured pores and channels in the crystal structure of these inorganic fillers can successfully provide tridimensional (3D) cages that have the adsorption capability of toxins including histamine (Selvam, Schwieger, & Dathe, 2018).

This research study deals with the development by electrospinning of active-scavenging electrospun films of PCL filled with either zeolite or SiO_2 microparticles to entrap histamine produced *in vitro* by both G- *Salmonella* Paratyphi A (*S.* Paratyphi A) and G+ *Staphylococcus aureus* (*S. aureus*). To achieve this objective, the inorganic microparticles were first incorporated into submicron PCL fibers by solution electrospinning and the resultant mats were thereafter thermally post-treated to produce continuous films. The morphological, mechanical, transparency, and histamine-binding capacity properties of the resultant zeolite- and SiO_2-containing PCL films were tested to ascertain their potential in active food packaging.

2. Materials and methods

2.1. Materials

PCL (reference 440744) with a weight-average molecular weight (M_W) of 80 kDa and a water content < 0.5% was obtained from Sigma-Aldrich S.A. (Madrid, Spain). Zeolite CFT-03 Sapo-34 with a chabazite topology was supplied by Tianjin Chemist Scientific, Ltd. (Tianjin, China). Hydrophobic pyrogenic SiO_2 nanostructured microparticles (HDK H18) with an average particle size of approximately 17 μm and a Brunauer–Emmett–Teller (BET) surface area of 170–230 m^2/g were obtained from Wacker Chemie Company (Munich, Germany). Further details about the morphology and characteristics of the microparticles of zeolite (Torres-Giner, Torres, Ferrándiz, Fombuena, & Balart, 2017) and SiO_2 (Lasprilla-Botero et al., 2018; Pardo-Figuerez, López-Córdoba, Torres-Giner, & Lagaron, 2018) can be found elsewhere.

Chloroform (288306), L-histidine monohydrochloride monohydrate (H8125) with a purity of ≥98%, pyridoxal hydrochloride (P9130), peptone (68971), nutrient broth (70122), acetonitrile (HPLC grade) (34998), sodium chloride (NaCl) (S9888), ethanol (493511), trichloroacetic acid (TCA) (T6399), sodium hydroxide (NaOH) (221465), diethyl ether (309966), potassium hydroxide (KOH) (1310-58-3), histamine dihydrochloride (PHR1357-500MG), Tryptic Soy Agar (22091) and benzoyl chloride (259950) were all purchased from Sigma-Aldrich S.A. 1-Butanol (131082.1612) was provided by Panreac S.A. (Barcelona, Spain). The foodborne bacteria *S. aureus* (ATCC 29213) and *S. parathypi A* (NCTC13) were gently provided by Recep Tayyip Erdoğan University (Rize, Turkey).

2.2. Electrospinning

The electrospinning solutions were prepared by dissolving 4 wt% PCL in a 75/25 (vol/vol) solvent mixture of chloroform/butanol under magnetic stirring at room temperature, that is, 23 °C. Once PCL was fully dissolved, either the zeolite or SiO_2 microparticles were added, in powder form, to the biopolymer solution at contents of 5 wt%, 10 wt%, 15 wt%, and 20 wt% with respect to the PCL weight fraction. The resultant dispersions were stirred for at least 12 h until homogenous suspensions were achieved.

The PCL suspensions were then transferred to a 12-mL plastic syringe connected through a polytetrafluoroethylene (PTFE) tube to a stainless steel needle (diameter 0.9 mm) and then processed by electrospinning using a pilot-plant Fluidnatek™ LE-500 device (Bioinicia S.L., Valencia, Spain). This device was operated in lab mode with only one emitter, scanning vertically towards a metallic plate covered with aluminum foil. The solutions were electrospun for 2 h, under a steady flow-rate of 3 mL/h, setting a voltage of 14 kV and a tip-to-collector distance of 15 cm. A solution of neat PCL was also processed in the same conditions as control. All experiments were performed at room conditions, that is, 23 °C and 40% relative humidity (RH), in a controlled environmental chamber.

2.3. Films preparation

The resultant electrospun PCL mats were thermally post-treated using a hydraulic press 4122-model from Carver, Inc. (Wabash, IN, USA). Annealing was carried out at various temperatures, that is, 45°C, 55°C, and 65°C, for an interval of 40 s, without pressure, based on previously optimized conditions.(Lasprilla-Botero et al., 2018)

2.4. Materials characterization

2.4.1. Solution properties

All biopolymer solutions were characterized in terms of viscosity, surface tension, and conductivity. The apparent viscosity (ηa) was determined at 100 s^{-1} using a rotational viscosity meter Visco BasicPlus L from Fungilab S.A. (San Feliu de Llobregat, Spain) equipped with a low-viscosity adapter (LCP). The surface tension was measured following the Wilhemy plate method using an EasyDyne K20 tensiometer from Krüss GmbH (Hamburg, Germany). The conductivity was evaluated using a conductivity meter XS Con6 from Lab-box (Barcelona, Spain). All measurements were carried out at room temperature in triplicate.

2.4.2. Film thickness and conditioning

Film thickness was measured with a digital micrometer series S00014, having ±0.001 mm accuracy, from Mitutoyo Corporation (Kawasaki, Japan) at three random positions. All the film samples were

158 equilibrated, before evaluation, in a desiccator at 0% RH containing dried silica gel at a constant
159 temperature of 23 °C for 1 week.

160 2.4.3. Electron microscopy

161 Scanning electron microscope (SEM) was used to evaluate the morphology of the zeolite and SiO_2
162 powders, the electrospun PCL fibers, and the cross-sections and surfaces of the resultant films. To
163 this end, a Hitachi S-4800 electron microscope (Tokyo, Japan) operating at an accelerating voltage
164 of 20 kV and a working distance of 8–10 mm was used. Film cross-sections of the samples were
165 previously prepared by cryofracture using liquid nitrogen. Prior to observation, all samples were fixed
166 to beveled holders using conductive double-sided adhesive tape, sputtered with a mixture of gold-
167 palladium under vacuum for 3 min. At least 20 SEM images were used to determine the average sizes
168 with ImageJ Launcher v 1.41 software.

169 Transmission electron microscopy (TEM) was performed to analyze the dispersion of the zeolite and
170 SiO_2 microparticles in the electrospun PCL fibers. A Jeol 1010 equipment from JEOL USA, Inc.
171 (Peabody, MA, USA), operating with an acceleration voltage of 80 kV, was employed. The nanofibers
172 were previously collected on a sandwich-type holder (Agar Scientific-G230, Agar Scientific Ltd,
173 Essex, UK) with a mesh size of 3.05 mm.

174 2.4.4. Transparency measurements

175 The light transmission of the films was determined in specimens of 50×30 mm^2 by quantifying the
176 absorption of light, using an ultraviolet–visible (UV–Vis) spectrophotometer UV-1800 Shimadzu
177 (Kyoto, Japan). The transparency value (T) of the films was calculated using **Equation 1** (Figueroa-
178 Lopez, Castro-Mayorga, Andrade-Mahecha, Cabedo, & Lagaron, 2018):
179

180 $$T = \frac{A_{600}}{L} \qquad (1)$$

181 Where A_{600} is the absorbance value at 600 nm and L is the film thickness (mm). Measurements were
182 performed in triplicate.

183 2.4.5. Mechanical tests

184 Tensile tests were carried out on the electrospun mat and films using a TA.XT Plus Universal Testing
185 Machine from Stable Micro Systems, Ltd (Surry, UK). Tests were performed according to ISO 527-
186 1:2012 on uniform rectangular strips with dimensions of 50×5 mm^2 using miniature tensile grips. The
187 cell load was 100 N, the grip distance was 10 mm, and the cross-head speed was 2 mm/min. At least
188 six samples of each material were tested at room temperature.

189 2.4.6. Histamine production and determination

190 Histamine production in culture medium was carried out following the method described by Klausen
191 & Huss (1987). Briefly, 2 g of peptone, 5 g of NaCl, 8.02 g of L-histidine monohydrochloride
192 monohydrate, and 5 mg of pyridoxal hydrochloride were added to 1000 mL of purified water. The
193 resultant solution was first adjusted to pH 6.0 with 1M KOH and, thereafter, sterilized at 121 °C for
194 15 min to obtained the so-called histidine amino acid decarboxylase solution. The two selected food
195 pathogens, that is, *S. aureus* and *S.* Paratyphi A*,* were then separately cultivated in nutrient broth
196 (70122) from Sigma-Aldrich S.A., having a concentration of 0.5 McFarland turbidity standard that is
197 equivalent to 1.45×10^7 colony forming units (CFU)/ml for *S. aureus* and 1.3×10^7 colony forming
198 units (CFU)/ml for *S.* Paratyphi A, for 24 h at 37 °C. Thus, 0.5 mL of each bacterial medium was
199 transferred separately to the tubes containing the histidine amino acid decarboxylase solution to allow
200 them to decarboxylate histidine. Film samples sizing 2×2 cm^2 were then immersed into the above-
201 prepared histidine amino acid decarboxylase solution containing the bacterial culture and the whole
202 suspension was stored for histamine production for 72 h at 37 °C. Thereafter, the film samples were
203 removed from the histamine-containing tubes and their surfaces were washed with ethanol to remove
204 the excess of non-binding components from the films. The films were allowed to dry under vacuum
205 at 23 °C for 2 h. Then, 2 mL of 6 vol% TCA was added to the control tubes, without the film samples,
206 for the histamine extraction control and all the tubes were centrifuged at 10,000 rpm for 10 min at 4
207 °C. The values of pH and the bacterial growth were also determined for each solution at the end of
208 the incubation period. pH values of each solution was determined by using a pH meter (Mettler Toledo

209 SG2-FK - SevenGo ™ pH meter, USA). Bacterial growth was also monitored parallel with histamine
210 production. For this, spread plate method was used and 0.1 mL of well-mixed diluted samples were
211 inoculated to Tryptic Soy Agar (Sigma-Aldrich, 22091) surface then, distributed the inoculum by
212 sterile spreader device aseptically. The petri dishes were incubated 24 h at 37 °C.
213 For the determination of the histamine entrapped in the films, the samples were dissolved in 4 mL of
214 chloroform and the resultant solutions were then passed through a 47-µm filter (Isolab Laborgeräte
215 GmbH, Wertheim, Germany). Thereafter, 4 mL of the solution was transferred to a new tube and 1
216 mL of 2 M NaOH and 40 µL of benzoyl chloride was added and vortexed for 40 s for benzylation.
217 The mixture was further allowed to stand at room temperature for 20 min in order to complete
218 benzylation, which was ended by adding 2 mL of saturated NaOH. Thus, the solution was extracted
219 with 4 mL of diethyl ether. The upper organic phase formed after the extraction process was
220 transferred to the tubes, the ether was evaporated by purging nitrogen gas at a pressure of 1.5 bar, and
221 the residues in the tube were dissolved in 1 mL of acetonitrile. The resultant suspension was filtered
222 again and then 1.5 mL of sample was transferred to amber vials with PTFE caps for chromatographic
223 analyses. The content of histamine in the film samples was determined by high-performance liquid
224 chromatography (HPLC, Agilent 1100 series, Agilent Technologies Hewlett-Packard-Strasse 8,
225 76337 Waldbronn, Germany) equipped with a diode array detector (DAD) and InfinityLab Poroshell
226 120 EC- C18 column. A standard solution of histamine dihydrochloride was prepared by dissolving
227 165.7 mg in 10 mL of ultrapure water and the final concentration of the free base was adjusted to 10
228 mg/mL. Derivatization of the standard solution was done in the above-mentioned conditions
229 described for the film samples. HPLC determination conditions were set at 254 nm using acetonitrile
230 and ultrapure water as the mobile phases. A calibration curve of histamine against peak area was
231 generated to measure the final histamine values (Y= 252222×X + 384.192; R^2 = 0.9996). The
232 percentage of entrapped histamine in the films was determined as the quantity of histamine obtained
233 in the dissolved films versus the produced histamine in the control sample without film. Tests were
234 performed in triplicate by each bacterial species.

235 *2.5. Statistical analysis*

The solution and mechanical properties as well as the histamine extraction were evaluated through analysis of variance (ANOVA) using STATGRAPHICS Centurion XVI v 16.1.03 from StatPoint Technologies, Inc. (Warrenton, VA, USA). Fisher's least significant difference (LSD) was used at the 95% confidence level ($p < 0.05$). Mean values and standard deviations were also determined.

3. Results and discussion

3.1. Solution properties

PCL was readily soluble in chloroform/butanol at 4 wt% and all the mineral microparticles were well dispersed in the polymer solutions prior and during the electrospinning process up to contents of 20 wt%. It is well known that the attained morphology during electrospinning is strongly dependent on a number of processing parameters (Li & Xia, 2004). **Table 1** gathers the values of viscosity, surface tension, and conductivity of the PCL solutions.

[Place Table 1 near here]

Among all the studied solution parameters, viscosity is the most important factor affecting the morphology of electrospun polymers and it is directly related to the polymer concentration and polymer's M_W (Ramakrishna, Fujihara, Teo, Lim, & Ma, 2005). The viscosity of the neat PCL solution was 0.7548 Pa·s, similar with that reported earlier by Beachley & Wen (2009), and the viscosity values of the PCL solutions were significantly higher as the content of both zeolite and SiO_2 microparticles increased. One can consider that this effect was produced due to the fact that the microparticles interaction became higher and the PCL molecules mobility lower with the increasing volume fraction of the suspended microparticles in the dispersion. At the highest filler contents, the viscosity increase was significantly lower in the case of the PCL dispersions with SiO_2 than zeolite, then suggesting a higher interaction of the latter microparticles with the biopolymer. For instance, whereas the PCL/SiO_2 20 wt% solution resulted in a viscosity of 1.8647 Pa·s, the solution with the same concentration of zeolite presented a value of 8.194 Pa·s. In terms of electrospinnability, it has been reported that relatively high viscosities are desirable to obtain uniform electrospun fibers from

biopolymers, however excessively high viscosities can yield low processability due to instabilities during processing (Sreekumar, Lemke, Moerschbacher, Torres-Giner, & Lagaron, 2017). In relation to surface tension, the neat PCL solution presented a value of 27.8 mN/m. One can observe that the presence of high zeolite contents reduced the surface tension up to values of 24.0 mN/m, whereas the silica microparticles increased the values up to 33.9 mN/m. The latter change can be ascribed to the high hydrophobicity of SiO_2 that can increase the surface energy, that is, the amount of intermolecular force created at the liquid surface, of the PCL solutions in chloroform (Lasprilla-Botero et al., 2018). Lower values of surface tension are habitually preferred during electrospinning since they can potentially increase the processability of biopolymers as it reduces the force needed to ungroup the assortment of molecules during the applied electric field (Geng, Kwon, & Jang, 2005). Finally, it can be observed that zeolite had a negligible effect on the conductivity of the PCL solution, showing values in the 0.01–0.02 μS/cm range. As opposite, the SiO_2 addition increased the PCL solution conductivity around 10 times, indicating that the these microparticles present certain ionic nature, which is another factor that may limit its processability by electrospinning (Tang, Abd-El-Aziz, Dong, Masuda, & Weder, 2014). In any case, although solution properties can anticipate processability issues during electrospinning, habitually it is difficult to elucidate the effect of a single property without considering the impact of the other ones (Torres-Giner, Wilkanowicz, Melendez-Rodriguez, & Lagaron, 2017).

3.2. Morphology of microparticles

Fiber diameter and shape can play a key role in the final properties of the electrospun materials and the films prepared from these. The morphology of the SiO_2 and zeolite microparticles was analyzed by SEM and **Figure 1** shows the micrographs of the as-received mineral powders. On the one hand, it is seen that SiO_2 was composed of surface micro-sized aggregates made of nanoparticles with an average diameter of approximately 60 nm (**Figure 1A**). The absorption performance and functionalization of the silica particle surface is usually attained by the high porosity formed as a result of the nanoparticles aggregates (Hien, Shirai, & Fuji, 2012). On the other, zeolite, which is

287 known to crystallize in a triclinic crystal system to form humidity ombohedral-shaped crystals (Li,
288 Li, Jiang, Tao, & Mai, 2013), was presented in the form of cubes with dimensions between 1–3 μm
289 and a bimodal particle size distribution (**Figure 1B**). The cage-like cavities of zeolite typically range
290 in the order of 3 Å to 15 Å, thus being not observable by SEM. This particular morphology confers
291 zeolite the ability of adsorbing or rebuffing molecules depending on their size, shape, and polarity
292 (Breck, Eversole, Milton, Reed, & Thomas, 1956; Kickelbick, 2003; Yuzay, Auras, Soto-Valdez, &
293 Selke, 2010).

294 [Place Figure 1 near here]

295 *3.3. Morphology of electrospun fibers*

296 The SEM micrographs of the electrospun PCL fibers containing different amounts of zeolite or silica
297 SiO_2 microparticles are shown in **Figure 2**. In **Figure 2A**, it can be observed that the neat PCL mat
298 was composed of round-like fibers having a smooth surface morphology without beads. The
299 electrospun fibers presented a dual distribution of sizes, which have been associated with the
300 formation of satellite drops during the breakup of the solution jet (Deitzel, Kleinmeyer, Harris, &
301 Beck Tan, 2001), having thick fibers with a mean diameter of 1039 ± 236 nm that coexisted with
302 nanofibers of 37 ± 3 nm. The high viscosity observed above for the solutions suggests that the
303 biopolymer presented sufficient chains entanglement to overcome the electrical charges during
304 electrospinning and fully stretch into bead-free fibers (Shahabadi, Kheradmand, Montazeri, & Ziaee,
305 2015). The SEM images of the electrospun mats of the SiO_2-containing PCL fibers are shown in
306 **Figures 2B-E**. At low SiO_2 contents, that is 5 wt% and 10 wt%, the electrospun fibers were relatively
307 similar to those observed for the neat PCL though their diameters were slightly lower. In particular,
308 the PCL/SiO_2 5 wt% presented a bimodal distribution with mean values of 802 ± 136 nm and 56 ± 5
309 nm whereas these values were 729 ± 102 nm and 55 ± 4 nm for the PCL/SiO_2 10 wt%, as respectively
310 seen in **Figures 2B** and **2C**. At 15 wt% SiO_2, however, the PCL fiber morphology was altered. **Figure**
311 **2D** shows that these composite fibers became corrugated, showing an unimodal distribution with a
312 mean diameter of 683 ± 121 nm, whereas some beaded regions along the fibers were formed. This

morphological change can be ascribed to a combined increase of viscosity and surface tension for the dispersions used for electrospinning. In this regard, Forouharshad et al. (2010) reported that, under the effect of surface tension, the high numbers of free solvent molecules in the solution come together into a spherical shape causing the formation of beads. In any case, the relatively high viscosities attained also prevented breakup of the jet due to an increased polymer chain entanglement that led to the formation of fibers instead of beads (Tarus, Fadel, Al-Oufy, & El-Messiry, 2016). In **Figure 2E**, showing the electrospun PCL fiber filled with the highest SiO_2 content, that is, 20 wt%, one can observe that the microparticles highly agglomerated and were located outside the fibers. As a result, the fiber diameter also decreased to values of 583 ± 112 nm. Similarly, Shin et al. (2013) reported that the diameter of electrospun PCL nanofibers containing SiO_2 microparticles decreased with the filler content increased.

[Place Figure 2 near here]

The electrospun zeolite-containing PCL mats are gathered in **Figures 2F-I**. Zeolite, even at the lowest content, induced a significant change on the fiber morphology. The electrospun PCL/zeolite 5 wt% mat, shown in **Figure 2F**, was composed of fibers having a bimodal distribution with sizes of 773 ± 136 nm and 51 ± 7 nm in which the thicker fibers also presented beaded regions. Although the incorporation of higher contents of zeolite tended to both slightly reduce fiber diameter and generate a unimodal distribution, it also increased the size and number of beaded regions. In particular, the mean diameters were 683 ± 115 nm, 585 ± 122 nm, and 475 ± 151 nm for the PCL fibers containing 10 wt% (**Figure 2G**), 15 wt% (**Figure 2H**), and 20 wt% (**Figure 2I**) of zeolite, respectively. The beaded regions observed in the fibers can be related to the higher size of the zeolite microparticles, which were in the size range of the electrospun PCL fiber diameters, and also to difficulties encountered during electrospinning due to the high viscosities of the dispersions. Moreover, Wang and Peng (2010) indicated that zeolite has the capability to hold heavy metal ions by its porous structure by which it easily forms aggregates. Similar results were also reported by Hwang et al. (2013), showing that the diameter of electrospun fibers of poly(butylene succinate) (PBS) decreased

considerably by the addition of zeolite whereas, when the mineral concentration increased above the optimal concentration, fibers were thicker and aggregated at the needle tip.

TEM was also performed on the composite PCL fibers in order to ascertain the dispersion of the SiO_2 and zeolite microparticles in the electrospun fibers. The distribution of the SiO_2 microparticles in the core of the electrospun fibers are illustrated in the TEM images included in **Figure 3A-B**. It can be seen that the SiO_2 microparticles were efficiently encapsulated in the fiber matrix though they also tended to agglomerate in certain regions. In the case of the zeolite-containing PCL fibers, shown in **Figure 3C-D**, the microparticles presented a lower degree of agglomeration at low contents. However, zeolite was excluded from the fibers at higher contents. An apparent good dispersion for both SiO_2 and zeolite was kept up to 10 wt% of mineral content, whereas bigger agglomerates were formed at 20 wt%. This can be ascribed to an inhomogeneous distribution of the mineral fillers due to solubility limits within the biopolymer matrix (Hwang et al., 2013; Torres-Giner & Lagaron, 2010). Similar morphologies were reported, for instance, by Mehrasa et al., 2016 when SiO_2 and zeolite nanoparticles were incorporated into electrospun polyvinyl alcohol (PVA)/collagen nanofibers.

[Place Figure 3 near here]

3.4. Morphology of electrospun composite films

The electrospun fibers mats were aimed to be turned into actual films by the application of thermal post-treatment at different temperatures, for a few seconds, since they can be more advantageous for application in food packaging. In order to ascertain the film-forming process, the cryofracture surfaces of the electrospun PCL mats were analyzed by SEM. **Figure 4** shows the cross-sections of the electrospun neat PCL mats prior to annealing (**Figure 4A**) and after post-treatment at 45 °C (**Figure 4B**), 55 °C (**Figure 4C**), and 65 °C (**Figure 4D**), all for 40 s and without pressure. It can be seen that at 45 °C, the electrospun PCL material preserved their original fiber-based morphology though the mat porosity was slighlty reduced. Annealing at 55 °C, interestingly, yielded a continuous film with a very low porosity, which has been ascribed to a packing rearrangement of the electrospun fibers (Cherpinski et al., 2017; Melendez-Rodriguez et al., 2018). Also, it is obviously seen that the

individual electrospun fibers coalesced and merged almost completely without losing their fibrilar morphology. At 65 °C, however, the SEM image revealed that the electrospun mat was melted due to PCL's T_m was exceeded, showing strong evidences of plastic deformation during fracture. As a result of annealing, the thicknesses of the electrospun PCL samples changed from approximately 200 μm, for the fibers mat, to around 60 μm, for the annealed films.

[Place Figure 4 near here]

Based on the above results, the electrospun composite fibers of PCL filled with SiO_2 or zeolite microparticles were subjected to annealing at 55 °C. The SEM images taken on the cross-sections of the resultant thermally post-treated electrospun materials are gathered in **Figure 5**. The resultant electrospun films presented a mean thickness of 60 ± 5 μm. **Figures 5A-D** show the electrospun SiO_2-containing PCL films where the contents of up to 15 wt% SiO_2 resulted in films with a similar fracture. The microparticles were clearly visible from the pouch-like opening shown in **Figures 5A** and **5B**, corresponding to the PCL/SiO_2 5 wt% and PCL/SiO_2 10 wt% films, respectively. In the cross-section of the PCL/SiO_2 15 wt% film, shown in **Figure 5C**, it is seen that several microparticles were finely dispersed in the electrospun PCL matrix as similarly reported by Lasprilla-Botero et al. (2018). At 20 wt% SiO_2, however, the particles were more agglomerated. As also previously described by Pardo-Figuerez et al. (2018), SiO_2 nanoparticles habitually tend to agglomerate in microparticles and also form large mineral aggregates due to the strong cohesive forces between their primary particles. The electrospun zeolite-containing PCL films are included in **Figures 5E-H**. Similar to the SiO_2 microparticles, zeolite was efficiently encapsulated and relatively well distributed in the electrospun PCL films up to contents of 15 wt%. In all these fracture surfaces, gathered in **Figures 5E-G**, cubic-shaped zeolite microparticles can be distinguished within the electrospun PCL matrix and it has been exhibited that the film morphology was successfully attained after annealing. In contrast, in **Figure 5H**, corresponding to the PCL/zeolite 20 wt% film, it can be observed that the fibers did not effectively coalesce due to the high content and size of zeolite.

[Place Figure 5 near here]

The visual properties of the films are also an important factor in terms of consumer acceptability. **Figure 6** shows the appearance of the electrospun films developed. Simple naked eye examination of this image indicated that annealing produced continuous PCL films with relatively high contact transparency properties, showing a *T* value of 12.6 ± 2.0. Only the PCL/zeolite 20 wt% sample resulted in an opaque film, having a *T* value of 18.5 ± 3.1, which can be ascribed to the fiber-based morphology observed in previous **Figure 5H**. This effect is due to the inherent opacity of the electrospun mats, which is composed of fibers placed randomly that generate a significant level of porosity and hence refract the light very strongly (Quiles-Carrillo et al., 2019). As opposite, the composite films containing 5–10 wt% mineral fillers showed a relative high transparency, presenting *T* values in the 11–14 range. This result indicates that the here-prepared electrospun composite PCL-based mats containing SiO_2 and zeolite microparticles up to contents of 15 wt% can be turned into actual films, which may be advantageous for active packaging applications.

[Place Figure 6 near here]

3.5. Mechanical properties of electrospun composite films

Figure 7 shows the representative tensile stress–strain curves for the electrospun PCL fibers and the annealed films made of neat PCL and PCL filled with different contents of SiO_2 and zeolite. All electrospun materials presented typical non-linear curves based on elastic deformation until they reach the yield point, the so-called elastic limit, from which plastic deformation occurred. The mechanical properties obtained from the curves are reported in **Table 2**. As seen from the table, the mechanical strength of the PCL nanofibers was very low, showing values of tensile modulus (*E*) and tensile strength at yield (σ_y) of 19.6 ± 6.1 MPa and 4.5 ± 0.8 MPa, respectively, whereas the average value of elongation at break (ε_b) was 183.9 ± 9.8 %. These values are consistent with those reported in literature for non-woven electrospun mats composed of PCL fibers with similar diameters (Croisier et al., 2012). This poor mechanical behavior is related to the high porosity of the electrospun materials. Indeed, fiber mats prepared by electrospinning present a percentage of porosity typically ranging from 70% to 90% (vol/vol) (Lowery, 2009). As opposite, the electrospun PCL film was

mechanically stronger and also slightly less ductile in comparison with the electrospun mat. In particular, the neat PCL film exhibited values of E and σ_y of 188.3 ± 10.1 MPa and 22.5 ± 3.4 MPa whereas the ε_b value was 162.5 ± 8.1 %. This mechanical enhancement can be mainly related to the improved homogeneity and reduced porosity attained in the electrospun sample after annealing. The mechanical performance observed in the electrospun films is relatively similar than that reported for melt-extruded PCL films, that is, E of 190 ± 6 MPa, σ_y of 14.2 ± 1.4 MPa, and ε_b > 550% (Averous, Moro, Dole, & Fringant, 2000), which can be considered a very elastic and tough material. The differences attained can be ascribed to the test conditions and sample orientation but also to interactions between the coalesced fibers in the electrospun film sample such as slip of fibers over one another, point bonding, alignment, etc. (Kim, Han, Park, & Kim, 2007). In this sense, previous results have indicated that thermal post-processing of the electrospun biopolymer fibers in a controlled manner can successfully generate materials with a more balanced mechanical performance than those prepared by conventional melting routes (Cherpinski et al., 2017; Melendez-Rodriguez et al., 2018).

[Place Figure 7 near here]

[Place Table 2 near here]

Incorporation of both fillers at the lowest contents, that is, 5 and 10 wt%, slightly improved the E and σ_y values but reduced ε_b, indicating the films became more rigid and less ductile. Also, the mechanical performance of the composite film produced at 15 wt% zeolite, that is, PCL/zeolite 15%, was still acceptable in terms of mechanical strength and ductility. However, the highest content of zeolite, that is, 20 wt%, and loading of SiO_2 of 15 wt% and 20 wt% resulted in film samples with a relatively low elastic limit and excessive brittleness. This effect can be related to both a phenomenon of particle agglomeration, previously observed in **Figure 3** during TEM analysis, and also to the high porosity remained in these electrospun annealed samples due to the difficulties of fibers to coalesce, as imaged in previous **Figure 5**. Therefore, the improved mechanical strength and toughness observed for the electrospun PCL films produced at low and moderate filler contents makes them suitable candidates for food packaging applications.

444 *3.6. Histamine-binding capacity of electrospun composite films*

445 The histamine entrapment performance of the electrospun composite films of PCL with SiO_2 and
446 zeolite microparticles was investigated by the culture media method, in which histamine-producing
447 bacteria were developed in a L-histidine amino acid decarboxylase solution in the presence of the film
448 samples. To this end, *S. aureus* (G+) and *S.* Paratyphi A (G-) were both tested to produce histamine
449 *in vitro*. These two bacteria were selected since they are among the most reported histamine producer
450 microorganisms in fermented salted fish and fishery products (Allen, 2004; Laganà et al., 2015;
451 Özogul et al., 2015). **Table 3** shows the amount of histamine entrapped for each electrospun film as
452 well as their binding capacity, which was determined by the percentage of entrapped amount of
453 histamine with respect to the total histamine produced in the media, for each bacterium. pH of each
454 soltion and bacterial growth parallel with histamine production after 72 h of incubation was shown in
455 the table. As seen from the table, both bacteria formed similar amounts of histamine, in the 0.7–0.8
456 mg/L range, being slightly higher in the case of *S.* Paratyphi A. This minor difference can be ascribed
457 to the fact that histamine is a competitive inhibitor of the pyruvoyl enzymes, which is encountered in
458 G- bacteria, but not of the pyridoxal phosphate enzymes that are found in G+ bacteria (De Las Rivas,
459 Rodríguez, Carrascosa, & Muñoz, 2008; Landete, De Las Rivas, Marcobal, & Muñoz, 2008).
460 Therefore, when *S. aureus* began to produce histamine *via* the enzyme group of pyruvoyl, the formed
461 histamine itself inhibited the formation of the pyruvoyl-dependent enzyme. The results showed that,
462 whereas the neat electrospun PCL film presented no histamine-binding capacity, all the composite
463 films showed increasing capacity with the filler loading. The zeolite-containing PCL films offered
464 significantly higher histamine-binding capacity than those composite films based on SiO_2
465 microparticles. For instance, the PCL/zeolite 5 wt% film sample was able to entrap similar
466 percentages of histamine than the PCL/SiO_2 20 wt%, that is, both values were approximately 80%
467 and 55% for *S. aureus* and *S.* Paratyphi A, respectively. This result suggests that, although both
468 mineral microparticles can successfully adsorb organic molecules and permanent gases by a volume
469 filling effect of their nanopores, zeolite is significantly more effective to entrap histamine. This
470 observation can be explained by the fact that its surface selectivity for hydrophilic and other polar

471 molecules is higher than that of SiO_2. The latter microparticles are known to be more selective for the
472 adsorption of organic molecules smaller than its limiting pore size so that they can be still a valuable
473 material for other active packaging applications (Melendez-Rodriguez et al., 2019) and also
474 detoxification therapies (Yantasee et al., 2010).

475 [Place Table 3 near here]

476 In this regard, Selvam et al. (2018) recently observed that Cuban zeolites present higher histamine-
477 binding capacity than Mexican ones due to their higher pore volume and lower particle sizes.
478 Similarly, Özogul et al. (2015) previously reported that histamine was strongly adsorbed onto natural
479 zeolite at pH values from 1 to 7. One can also observe that the binding capacity of both fillers was
480 higher for *S. aureus* than for *S*. Paratyphi A. This observation can be then related to slighlt variations
481 of the pH level of the culture media due to the products, by-products, and waste compounds such as
482 organic acids produced by the bacteria growth and metabolism (Sánchez-Clemente et al., 2018). The
483 pH value was initially adjusted to 6.0 to avoid alkalization by the formed ammonia but during the
484 entrapment test, as shown in the table, it slighly decreased to values around 5.5. and 5.8 for *S. aureus*
485 than for *S.* Paratyphi A., respectively. Indeed, zeolite and SiO_2 both show different binding capability
486 as a function of pH. For instance, the natural zeolite's efficiency to remove histamine is typically
487 achieved in the pH range 5–6 since at these conditions the histamine species are found in a dissociated
488 ammonium (NH^{4+}) form so that its ion-exchange with the cations in the zeolite structure can
489 successfully occur (Moshoeshoe, Nadiye-Tabbiruka, & Obuseng, 2017). This observation further
490 supports the higher histamine-binding performance achieved for zeolite in the electrospun film
491 samples. Bacterial growth of each group was monitored after 72 h of incubation. Initial count for *S.*
492 *aureus* was 1.45×10^7 CFU/ml and for *S.* Paratyphi A was 1.3×10^7 CFU/ml. After the incubation
493 period, *S. aureus* was multiplied up to 14.04×10^7 while *S.* Paratyphi A was 16.32×10^7. The presence
494 of either both different levels of SiO_2 and zeolite including PCL electrospun films or neat PCL
495 electrospun films did not affect the bacterial growth significiantly.Our results also similar with the
496 (Hanim, Malek, & Ibrahim, 2016; Krokowicz et al., 2015; Yao et al., 2019) indicate that both zeolite
497 and silica itself have no antimicrobial activity and correlated to (Gokdogan et al., 2012), reported that

zeolite in certain concentrations stimulate bacterial growth. This results demonstrate that proper amounts of zeolite and silica including PCL electrospun films are recommended to use removing histamine from the fishery products.

4. Conclusions

Histamine, a biogenic amine, is a heat-stable compound and its removal from fish and fishery products is currently a technological challenge. The present study evaluated the incorporation of nanostructured SiO_2 and zeolite microparticles into submicron PCL fibers by solution electrospinning in order to develop highly effective materials to entrap histamine. The resultant electrospun composite mats were thermally post-treated to generate continuous and transparent films of more application interest in food packaging. The mechanical analysis performed showed that the electrospun PCL fiber mats could be effectively turned into actual films with similar performance than their counterpart melt-extruded films. Finally, the electrospun zeolite-containing PCL films showed high histamine-binding capacity formed in vitro by *S. aureus* and *S.* Paratyphi A, even at the lowest mineral content, which was ascribed to its porous-like surface characteristics and more optimal selectivity for the adsorption of hydrophilic and polar molecules. Therefore, the biopolymer composite films developed herein show a great deal of potential for histamine entrapment in fish and fishery products in active packaging applications.

Acknowledgments

This research was funded by the Spanish Ministry of Science, Innovation, and Universities (MICIU) program number AGL2015-63855-C2-1-R and by the EU H2020 YPACK project (reference number 773872). The authors also thank the Republic of Turkey Ministry of Agriculture and Forestry General Directorate of Agricultural Research and Policies (TAGEM) and Central Fisheries Research Institute (SUMAE) for funding support through the projects TAGEM/HSGYAD/14/A05/P05/70 and TAGEM/HSGYAD/17/A03/P05/133. Figueroa-Lopez is a recipient of a Santiago Grisolía (GRISOLIAP/2017/101) grant of the Generalitat Valenciana (GVA) and Torres-Giner is on a Juan de la Cierva–Incorporación contract (IJCI-2016-29675) from MICIU.

References

Ahmed, O. (2019). Histamine and other biogenic amines formation in canned tuna fish inoculated with *Morganella morganii* or *Proteus mirabilis* in determining food safety during temperature abuse. *Nutrition and Food Toxicology*, *3*(4), 690–700.

Allen, D. G. (2004). *Regulatory Control Of Histamine Production In North Carolina Havested Mahi-Mahi (Coryphaena hippurus) and Yellowfin Tuna (Thunnus albacares): A Haccp-Based Industry Survey*. North Carolina State University.

Alp-Erbay, E., Dağtekin, B. B. (Gözü), Türe, M., Yeşilsu, A. F., & Torres-Giner, S. (2017). Quality improvement of rainbow trout fillets by whey protein isolate coatings containing electrospun poly(ε-caprolactone) nanofibers with *Urtica dioica* L. extract during storage. *Lwt*, *78*(14), 340–351. http://doi.org/10.1016/j.lwt.2017.01.002

Alp-Erbay, E., Yeşilsu, A. F., & Türe, M. (2019). Fish gelatin antimicrobial electrospun nanofibers for active food-packaging applications. *Journal of Nano Research*, *56*, 80–97. http://doi.org/10.4028/www.scientific.net/JNanoR.56.80

Averous, L., Moro, L., Dole, P., & Fringant, C. (2000). Properties of thermoplastic blends: Starch-polycaprolactone. *Polymer*, *41*(11), 4157–4167. http://doi.org/10.1016/S0032-3861(99)00636-9

Beachley, V., & Wen, X. (2009). Effect of electrospinning parameters on the nanofiber diameter and length. *Materials Science and Engineering C*, *29*(3), 663–668. http://doi.org/10.1016/j.msec.2008.10.037

Breck, D. W., Eversole, W. G., Milton, R. M., Reed, T. B., & Thomas, T. L. (1956). The properties of a new synthetic zeolite, type A. *Journal of the American Chemical Society*, *78*(1), 5963–5971.

Chang, S. C., Kung, H. F., Chen, H. C., Lin, C. Saint, & Tsai, Y. H. (2008). Determination of histamine and bacterial isolation in swordfish fillets (*Xiphias gladius*) implicated in a food borne poisoning. *Food Control*, *19*(1), 16–21. http://doi.org/10.1016/j.foodcont.2007.01.005

Cherpinski, A., Torres-Giner, S., Cabedo, L., & Lagaron, J. M. (2017). Post-processing optimization of electrospun submicron poly(3-hydroxybutyrate) fibers to obtain continuous films of interest in food packaging applications. *Food Additives and Contaminants - Part A Chemistry, Analysis, Control, Exposure and Risk Assessment*, *34*(10), 1817–1830. http://doi.org/10.1080/19440049.2017.1355115

Croisier, F., Duwez, A. S., Jérôme, C., Léonard, A. F., Van Der Werf, K. O., Dijkstra, P. J., & Bennink, M. L. (2012). Mechanical testing of electrospun PCL fibers. *Acta Biomaterialia*, *8*(1), 218–224. http://doi.org/10.1016/j.actbio.2011.08.015

De Las Rivas, B., Rodríguez, H., Carrascosa, A. V., & Muñoz, R. (2008). Molecular cloning and functional characterization of a histidine decarboxylase from *Staphylococcus capitis*. *Journal of Applied Microbiology*, *104*(1), 194–203. http://doi.org/10.1111/j.1365-2672.2007.03549.x

Deitzel, J. M., Kleinmeyer, J., Harris, D., & Beck Tan, N. C. (2001). The effect of processing variables on the morphology of electrospun nanofibers and textiles. *Polymer*, *42*(2001), 261–272.

European Communities. (1991). *Council Directive 91/493/EEC of 22 July 1991 laying down the health conditions for the production and the placing on the market of fishery products*.

Figueroa-Lopez, K., Castro-Mayorga, J., Andrade-Mahecha, M., Cabedo, L., & Lagaron, J. (2018). Antibacterial and Barrier Properties of Gelatin Coated by Electrospun Polycaprolactone Ultrathin Fibers Containing Black Pepper Oleoresin of Interest in Active Food Biopackaging Applications. *Nanomaterials*, *8*(4), 199. http://doi.org/10.3390/nano8040199

Filipczak, K., Janik, I., Kozicki, M., Ulanski, P., Rosiak, J. M., Pajewski, L. A., … Lewandowska-Szumiel, M. (2005). Porous polymeric scaffolds for bone regeneration. *E-Polymers*, (011), 1–13.

Forouharshad, M., Saligheh, O., Arasteh, R., & Farsani, R. E. (2010). Manufacture and characterization of poly (butylene terephthalate) nanofibers by electrospinning. *Journal of Macromolecular Science, Part B: Physics*, *49*(4), 833–842. http://doi.org/10.1080/00222341003609377

Geng, X., Kwon, O. H., & Jang, J. (2005). Electrospinning of chitosan dissolved in concentrated acetic acid solution. *Biomaterials*, *26*(27), 5427–5432. http://doi.org/10.1016/j.biomaterials.2005.01.066

Geornaras, I., Dykes, G. A., & Holy, A. Von. (1995). Biogenic amine formation by poultry-associated spoilage and pathogenic bacteria. *Letters in Applied Microbiology*, *21*, 164–166. http://doi.org/https://doi.org/10.1111/j.1472-765X.1995.tb01032.x

Gilbert, R. J., Hobbs, G., Murray, C. K., Cruickshank, J. G., & Young, S. E. (1980). Scombrotoxic fish poisoning: features of the first 50 incidents to be reported in Britain (1976-9). *British Medical Journal*, *281*(6232), 71–72.

Gokdogan, S., Özogul, Y., Kuley, E., Özogul, F., Kacar, C., & Ucar, Y. (2012). The influences of natural zeolite (cliptinolite) on ammonia and biogenic amine formation by foodborne pathogen. *Journal of Food Science*, *77*(8), 452–457. http://doi.org/10.1111/j.1750-3841.2012.02822.x

Hanim, S. A. M., Malek, N. A. N. N., & Ibrahim, Z. (2016). Amine-functionalized, silver-exchanged zeolite NaY: Preparation, characterization and antibacterial activity. *Applied Surface Science*, *360*, 121–130. http://doi.org/10.1016/j.apsusc.2015.11.010

Hernández-Herrero, M. M., Roig-Sagués, A. X., Rodríguez-Jerez, J. J., & Mora-Ventura, T. M. (1999). Halotolerant and halophilic histamine-forming bacteria isolated during the ripening of salted anchovies (*Engraulis encrasicholus*). *Journal of Food Protection*, *62*(5), 509–514. http://doi.org/10.4315/0362-028X-62.5.509

Hien, T. T. T., Shirai, T., & Fuji, M. (2012). Mechanical modification of silica powders. *Journal of the Ceramic Society of Japan*, *120*(1406), 429–435. http://doi.org/10.2109/jcersj2.120.429

Hungerford, J. M. (2010). Scombroid poisoning: A review. *Toxicon*, *56*(2), 231–243. http://doi.org/10.1016/j.toxicon.2010.02.006

599 Huwig, A., Freimund, S., Käppeli, O., & Dutler, H. (2001). Mycotoxin detoxication of animal feed
600 by different adsorbents. *Toxicology Letters*, *122*(2), 179–188. http://doi.org/10.1016/S0378-
601 4274(01)00360-5

602 Hwang, S. Y., Yoon, W. J., Yun, S. H., Yoo, E. S., Kim, T. H., & Im, S. S. (2013). Fabrication of
603 superabsorbent ultrathin nanofibers using mesoporous materials for antimicrobial drug-delivery
604 applications. *Macromolecular Research*, *21*(11), 1281–1288. http://doi.org/10.1007/s13233-
605 013-1178-3

606 Jin, G., Prabhakaran, M. P., Kai, D., Annamalai, S. K., Arunachalam, K. D., & Ramakrishna, S.
607 (2013). Tissue engineered plant extracts as nanofibrous wound dressing. *Biomaterials*, *34*(3),
608 724–734. http://doi.org/10.1016/j.biomaterials.2012.10.026

609 Kickelbick, G. (2003). Concepts for the incorporation of inorganic building blocks into organic
610 polymers on a nanoscale. *Progress in Polymer Science (Oxford)*, *28*(1), 83–114.
611 http://doi.org/10.1016/S0079-6700(02)00019-9

612 Kim, G. H., Han, H., Park, J. H., & Kim, W. D. (2007). An applicable electrospinning process for
613 fabricating a mechanically improved nanofiber mat. *Polymer Engineering & Science*, *47*(5),
614 707–712. http://doi.org/10.1002/pen.20744

615 Kimura, B., Konagaya, Y., & Fujii, T. (2001). Histamine formation by *Tetragenococcus muriaticus*,
616 a halophilic lactic acid bacterium isolated from fish sauce. *International Journal of Food*
617 *Microbiology*, *70*(1–2), 71–77. http://doi.org/10.1016/S0168-1605(01)00514-1

618 Klausen, N. K., & Huss, H. H. (1987). Growth and histamine production by *Morganella morganii*
619 under various temperature conditions. *International Journal of Food Microbiology*, *5*(2), 147–
620 156. http://doi.org/10.1016/0168-1605(87)90032-8

621 Krokowicz, L., Tomczak, H., Bobkiewicz, A., Mackiewicz, J., Marciniak, R., Drews, M., &
622 Banasiewicz, T. (2015). *In vitro* studies of antibacterial and antifungal wound dressings
623 comprising H_2TiO_3 and SiO_2 nanoparticles. *Polish Journal of Microbiology*, *64*(2), 137–142.

624 Kuley, E., Durmus, M., Balikci, E., Ucar, Y., Regenstein, J. M., & Özoğul, F. (2017). Fish spoilage
625 bacterial growth and their biogenic amine accumulation: Inhibitory effects of olive by-products.
626 *International Journal of Food Properties*, *20*(5), 1029–1043.
627 http://doi.org/10.1080/10942912.2016.1193516

628 Kuley, E., & Özogul, F. (2011). Synergistic and antagonistic effect of lactic acid bacteria on tyramine
629 production by food-borne pathogenic bacteria in tyrosine decarboxylase broth. *Food Chemistry*,
630 *127*(3), 1163–1168. http://doi.org/10.1016/j.foodchem.2011.01.118

631 Kung, H. F., Wang, T. Y., Huang, Y. R., Lin, C. Saint, Wu, W. S., Lin, C. M., & Tsai, Y. H. (2009).
632 Isolation and identification of histamine-forming bacteria in tuna sandwiches. *Food Control*,
633 *20*(11), 1013–1017. http://doi.org/10.1016/j.foodcont.2008.12.001

634 Laganà, P., Caruso, G., Barone, C., Caruso, G., Parisi, S., Melcarne, L., … Santi Delia, A. (2015).
635 *Microbial Toxins and Related Contamination in the Food Industry*. Italy: Springer.
636 http://doi.org/10.1007/978-3-319-20559-5

637 Lakshmanan, R., Shakila, R. J., & Jeyasekaran, G. (2002). Survival of amine-forming bacteria during
638 the ice storage of fish and shrimp. *Food Microbiology*, *19*(6), 617–625.
639 http://doi.org/10.1006/fmic.2002.0481

640 Landete, J. M., De Las Rivas, B., Marcobal, A., & Muñoz, R. (2008). Updated molecular knowledge
641 about histamine biosynthesis by bacteria. *Critical Reviews in Food Science and Nutrition*, *48*(8),
642 697–714. http://doi.org/10.1080/10408390701639041

643 Lasprilla-Botero, J., Torres-Giner, S., Pardo-Figuerez, M., Álvarez-Láinez, M., & Lagaron, J. M.
644 (2018). Superhydrophobic bilayer coating based on annealed electrospun ultrathin poly(ε-
645 caprolactone) fibers and electrosprayed nanostructured silica microparticles for easy emptying
646 packaging applications. *Coatings*, *8*(5), 173. http://doi.org/10.3390/coatings8050173

647 Lehane, L., & Olley, J. (2000). Histamine fish poisoning revisited. *International Journal of Food*
648 *Microbiology*, *58*(2000), 1–37. http://doi.org/10.1016/S0168-1605(00)00296-8

649 Li, D., & Xia, Y. (2004). Electrospinning of nanofibers: Reinventing the wheel? *Advanced Materials*,
650 *16*(14), 1151–1170. http://doi.org/10.1002/adma.200400719

651 Li, M., Li, G., Jiang, J., Tao, Y., & Mai, K. (2013). Preparation, antimicrobial, crystallization and
652 mechanical properties of nano-ZnO-supported zeolite filled polypropylene random copolymer
653 composites. *Composites Science and Technology*, *81*, 30–36.
654 http://doi.org/10.1016/j.compscitech.2013.03.020

655 López-Sabater, E. I., Rodríguez-Jerez, J. J., Roig-Sagués, A. X., & Teresa Mora-Ventura, M. A.
656 (1994). Bacteriological quality of tuna fish (*Thunnus thynnus*) destined for canning: Effect of
657 tuna handling on presence of histidine decarboxylase bacteria and histamine level. *Journal of*
658 *Food Protection*, *57*(4), 318–323. http://doi.org/10.4315/0362-028X-57.4.318

659 Lowery, J. L. (2009). *Characterization and Modification of Porosity in Electrospun Polymeric*
660 *Materials for Tissue Engineering Applications*. *Chemical Engineering*. University of Kentucky.

661 Mehrasa, M., Anarkoli, A. O., Rafienia, M., Ghasemi, N., Davary, N., Bonakdar, S., … Salamat, M.
662 R. (2016). Incorporation of zeolite and silica nanoparticles into electrospun PVA/collagen
663 nanofibrous scaffolds: The influence on the physical, chemical properties and cell behavior.
664 *International Journal of Polymeric Materials and Polymeric Biomaterials*, *65*(9), 457–465.
665 http://doi.org/10.1080/00914037.2015.1129958

666 Melendez-Rodriguez, B., Castro-Mayorga, J. L., Reis, M. A. M., Sammon, C., Cabedo, L., Torres-
667 Giner, S., & Lagaron, J. M. (2018). Preparation and characterization of electrospun food
668 biopackaging films of poly(3-hydroxybutyrate-co-3-hydroxyvalerate) derived from fruit pulp
669 biowaste. *Frontiers in Sustainable Food Systems*, *2*(July), 38.
670 http://doi.org/10.3389/fsufs.2018.00038

671 Melendez-Rodriguez, B., Figueroa-Lopez, K. J., Bernardos, A., Martínez-Máñez, R., Cabedo, L.,
672 Torres-Giner, S., & Lagaron, J. M. (2019). Electrospun antimicrobial films of poly(3-
673 hydroxybutyrate-co-3-hydroxyvalerate) containing eugenol essential oil encapsulated in
674 mesoporous silica nanoparticles. *Nanomaterials*, *9*(2), 227. http://doi.org/10.3390/nano9020227

675 Mohamed, R. M., & Yusoh, K. (2015). A review on the recent research of polycaprolactone (PCL).
676 *Advanced Materials Research*, *1134*, 249–255.
677 http://doi.org/10.4028/www.scientific.net/AMR.1134.249

678 Moshoeshoe, M., Nadiye-Tabbiruka, M. S., & Obuseng, V. (2017). A review of chemistry, structure,
679 properties and applications of zeolites. *American Journal of Materials Science*, *7*(5), 191–221.
680 http://doi.org/10.5923/j.materials.20170705.12

681 Murray, C. K., Hobbs, G., & Gilbert, R. J. (1982). Scombrotoxin and scombrotoxin-like poisoning
682 from canned fish. *Journal of Hygiene*, *88*(2), 215–220.
683 http://doi.org/10.1017/S002217240007008X

684 Naila, A., Flint, S., Fletcher, G., Bremer, P., & Meerdink, G. (2010). Control of biogenic amines in
685 food - existing and emerging approaches. *Journal of Food Science*, *75*(7).
686 http://doi.org/10.1111/j.1750-3841.2010.01774.x

687 Nei, D. (2014). Evaluation of non-bacterial factors contributing to histamine accumulation in fish
688 fillets. *Food Control*, *35*(1), 142–145. http://doi.org/10.1016/j.foodcont.2013.06.037

689 Özogul, F., Kacar, Ç., & Hamed, I. (2015). Inhibition effects of carvacrol on biogenic amines
690 formation by common food-borne pathogens in histidine decarboxylase broth. *LWT - Food*
691 *Science and Technology*, *64*(1), 50–55. http://doi.org/10.1016/j.lwt.2015.05.027

692 Pardo-Figuerez, M., López-Córdoba, A., Torres-Giner, S., & Lagaron, J. (2018). Superhydrophobic
693 bio-coating made by co-continuous electrospinning and electrospraying on polyethylene
694 terephthalate films proposed as easy emptying transparent food packaging. *Coatings*, *8*(10), 364.
695 http://doi.org/10.3390/coatings8100364

696 Quiles-Carrillo, L., Montanes, N., Lagaron, J., Balart, R., & Torres-Giner, S. (2019). Bioactive
697 multilayer polylactide films with controlled release capacity of gallic acid accomplished by
698 incorporating electrospun nanostructured coatings and interlayers. *Applied Sciences*, *9*(3), 533.
699 http://doi.org/10.3390/app9030533

700 Ramakrishna, S., Fujihara, K., Teo, W.-E., Lim, T.-C., & Ma, Z. (2005). *An introduction to*
701 *electrospinning and nanofibers*. World Scientific. http://doi.org/10.1142/5894

702 Sánchez-Clemente, R., Igeño, M. I., Población, A. G., Guijo, M. I., Merchán, F., & Blasco, R. (2018).
703 Study of pH changes in media during bacterial growth of several environmental strains.
704 *Proceedings*, *2*(20), 1297. http://doi.org/10.3390/proceedings2201297

705 Satomi, M. (2016). Effect of histamine-producing bacteria on fermented fishery products. *Food*
706 *Science and Technology Research*, *22*(1), 1–21. http://doi.org/10.3136/fstr.22.1

707 Selvam, T., Schwieger, W., & Dathe, W. (2018). Histamine-binding capacities of different natural
708 zeolites: A comparative study. *Environmental Geochemistry and Health*, 1–9.
709 http://doi.org/10.1007/s10653-018-0129-5

710 Shahabadi, S. M. S., Kheradmand, A., Montazeri, V., & Ziaee, H. (2015). Effects of process and
711 ambient parameters on diameter and morphology of electrospun polyacrylonitrile nanofibers.
712 *Polymer Science Series A*, *57*(2), 155–167. http://doi.org/10.1134/S0965545X15020157

Shalaby, A. R. (1996). Significance of biogenic amines to food safety and human health. *Food Research International*, *29*(7), 675–690. http://doi.org/10.1016/S0963-9969(96)00066-X

Shin, K., Koh, Y., & Kim, H. (2013). Synthesis and characterization of drug-loaded poly(-caprolactone)/silica hybrid nanofibrous scaffolds. *Journal OfNanomaterials*, *2013*(5), 1–12.

Showkat, A. M., Zhang, Y. P., Min, S. K., Gopalan, A. I., Reddy, K. R., & Lee, K. P. (2007). Analysis of heavy metal toxic ions by adsorption onto amino-functionalized ordered mesoporous silica. *Bulletin of the Korean Chemical Society*, *28*(11), 1985–1992. http://doi.org/10.5012/bkcs.2007.28.11.1985

Simon, S. S., & Sanjeev, S. (2007). Prevalence of enterotoxigenic *Staphylococcus aureus* in fishery products and fish processing factory workers. *Food Control*, *18*(12), 1565–1568. http://doi.org/10.1016/j.foodcont.2006.12.007

Sreekumar, S., Lemke, P., Moerschbacher, B. M., Torres-Giner, S., & Lagaron, J. M. (2017). Preparation and optimization of submicron chitosan capsules by water-based electrospraying for food and bioactive packaging applications. *Food Additives and Contaminants - Part A Chemistry, Analysis, Control, Exposure and Risk Assessment*, *34*(10), 1795–1806. http://doi.org/10.1080/19440049.2017.1347284

Sridhar, R., Ravanan, S., Venugopal, J. R., Sundarrajan, S., Pliszka, D., Sivasubramanian, S., … Ramakrishna, S. (2014). Curcumin-and natural extract-loaded nanofibres for potential treatment of lung and breast cancer: In vitro efficacy evaluation. *Journal of Biomaterials Science, Polymer Edition*, *25*(10), 985–998. http://doi.org/10.1080/09205063.2014.917039

Stratton, J. E., Hutkins, R. W., & Taylor, S. L. (1991). Biogenic amines in cheese and other fermented foods: A review. *Journal of Food Protection*, *54*(6), 460–470. http://doi.org/10.4315/0362-028X-54.6.460

Tang, B. Z., Abd-El-Aziz, A. S., Dong, J., Masuda, T., & Weder, C. (2014). *Electrospinning Principles, Practice and Possibilities*. (R. M. Geoffrey, Ed.). RSC Polymer Chemistry. Retrieved from , www.rsc.org

Tapingkae, W., Parkin, K. L., Tanasupawat, S., Kruenate, J., Benjakul, S., & Visessanguan, W. (2010). Whole cell immobilisation of natrinema gari BCC 24369 for histamine degradation. *Food Chemistry*, *120*(3), 842–849. http://doi.org/10.1016/j.foodchem.2009.11.025

Tarus, B., Fadel, N., Al-Oufy, A., & El-Messiry, M. (2016). Effect of polymer concentration on the morphology and mechanical characteristics of electrospun cellulose acetate and poly (vinyl chloride) nanofiber mats. *Alexandria Engineering Journal*, *55*(3), 2975–2984. http://doi.org/10.1016/j.aej.2016.04.025

Taylor, & Eitenmiller, R. R. (1986). *Histamine food poisoning: Toxicology and clinical aspects*. *Critical Reviews in Toxicology* (Vol. 17). http://doi.org/10.3109/10408448609023767

Taylor, J. M., Smith, S. C., & Calaby, J. H. (1985). Histamine poisoning associated with fish, cheese,, and other foods. Retrieved from http://www.jstor.org/stable/1381248

Torres-Giner, S., Echegoyen, Y., Teruel-Juanes, R., Badia, J., Ribes-Greus, A., & Lagaron, J. (2018).

751 Electrospun poly(ethylene-co-vinyl alcohol)/graphene nanoplatelets composites of interest in
752 intelligent food packaging applications. *Nanomaterials*, *8*(10), 745.
753 http://doi.org/10.3390/nano8100745

754 Torres-Giner, S., & Lagaron, J. M. (2010). Zein-based ultrathin fibers containing ceramic nanofillers
755 obtained by electrospinning. i. morphology and thermal properties. *Journal of Applied Polymer*
756 *Science*, *118*(2010), 778–789. http://doi.org/10.1002/app.32180

757 Torres-Giner, S., Martinez-Abad, A., & Lagaron, J. M. (2014). Zein-based ultrathin fibers containing
758 ceramic nanofillers obtained by electrospinning. II. Mechanical properties, gas barrier, and
759 sustained release capacity of biocide thymol in multilayer polylactide films. *Journal of Applied*
760 *Polymer Science*, *131*(18), 9270–9276. http://doi.org/10.1002/app.40768

761 Torres-Giner, S., Perez-Masia, R., & Lagaron, J. M. (2016). A Review on electrospun polymer
762 nanostructures as advanced bioactive platforms. *Polymer Engineerinig and Science*, *56*(5), 500–
763 527. http://doi.org/10.1002/pen

764 Torres-Giner, S., Torres, A., Ferrándiz, M., Fombuena, V., & Balart, R. (2017). Antimicrobial activity
765 of metal cation-exchanged zeolites and their evaluation on injection-molded pieces of bio-based
766 high-density polyethylene. *Journal of Food Safety*, *37*(4), 1–12.
767 http://doi.org/10.1111/jfs.12348

768 Torres-Giner, S., Wilkanowicz, S., Melendez-Rodriguez, B., & Lagaron, J. M. (2017).
769 Nanoencapsulation of aloe vera in synthetic and naturally occurring polymers by
770 electrohydrodynamic processing of interest in food technology and bioactive packaging.
771 *Journal of Agricultural and Food Chemistry*, *65*(22), 4439–4448.
772 http://doi.org/10.1021/acs.jafc.7b01393

773 USFDA-CFSAN. (2011). *Fish and Fishery Products Hazards and Controls Guidance*. *Department*
774 *of Health and Human Services Public Health Service Food and Drug Administration Center for*
775 *Food Safety and Applied Nutrition Office of Food Safety*.

776 Visciano, P., Schirone, M., Tofalo, R., & Suzzi, G. (2012). Biogenic amines in raw and processed
777 seafood. *Frontiers in Microbiology*, *3*(188), 1–10. http://doi.org/10.3389/fmicb.2012.00188

778 Wang, S., & Peng, Y. (2010). Natural zeolites as effective adsorbents in water and wastewater
779 treatment. *Chemical Engineering Journal*, *156*(1), 11–24.
780 http://doi.org/10.1016/j.cej.2009.10.029

781 Wang, X., Zhao, H., Turng, L. S., & Li, Q. (2013). Crystalline morphology of electrospun poly(ε-
782 caprolactone) (PCL) nanofibers. *Industrial and Engineering Chemistry Research*, *52*(13), 4939–
783 4949. http://doi.org/10.1021/ie302185e

784 Woodruff, M. A., & Hutmacher, D. W. (2010). The return of a forgotten polymer - Polycaprolactone
785 in the 21st century. *Progress in Polymer Science (Oxford)*, *35*(10), 1217–1256.
786 http://doi.org/10.1016/j.progpolymsci.2010.04.002

787 Yantasee, W., Rutledge, R. D., Chouyyok, W., Sukwarotwat, V., Orr, G., Warner, C. L., …
788 Addleman, R. S. (2010). Functionalized nanoporous silica for the removal of heavy metals from

789 biological systems: Adsorption and application. *ACS Applied Materials and Interfaces*, *2*(10),
790 2749–2758. http://doi.org/10.1021/am100616b

791 Yao, G., Lei, J., Zhang, W., Yu, C., Sun, Z., Zheng, S., & Komarneni, S. (2019). Antimicrobial
792 activity of X zeolite exchanged with Cu^{2+} and Zn^{2+} on *Escherichia coli* and *Staphylococcus*
793 *aureus*. *Environmental Science and Pollution Research*, *26*(3), 2782–2793.
794 http://doi.org/10.1007/s11356-018-3750-z

795 Yuzay, I. E., Auras, R., Soto-Valdez, H., & Selke, S. (2010). Effects of synthetic and natural zeolites
796 on morphology and thermal degradation of poly(lactic acid) composites. *Polymer Degradation*
797 *and Stability*, *95*(9), 1769–1777. http://doi.org/10.1016/j.polymdegradstab.2010.05.011

798 Zarei, M., Maktabi, S., & Ghorbanpour, M. (2012). Prevalence of *Listeria monocytogenes*, *Vibrio*
799 *parahaemolyticus*, *Staphylococcus aureus*, and *Salmonella* spp. in seafood products using
800 multiplex polymerase chain reaction. *Foodborne Pathogens and Disease*, *9*(2), 108–112.
801 http://doi.org/10.1089/fpd.2011.0989

802

803 **Figure captions**

804 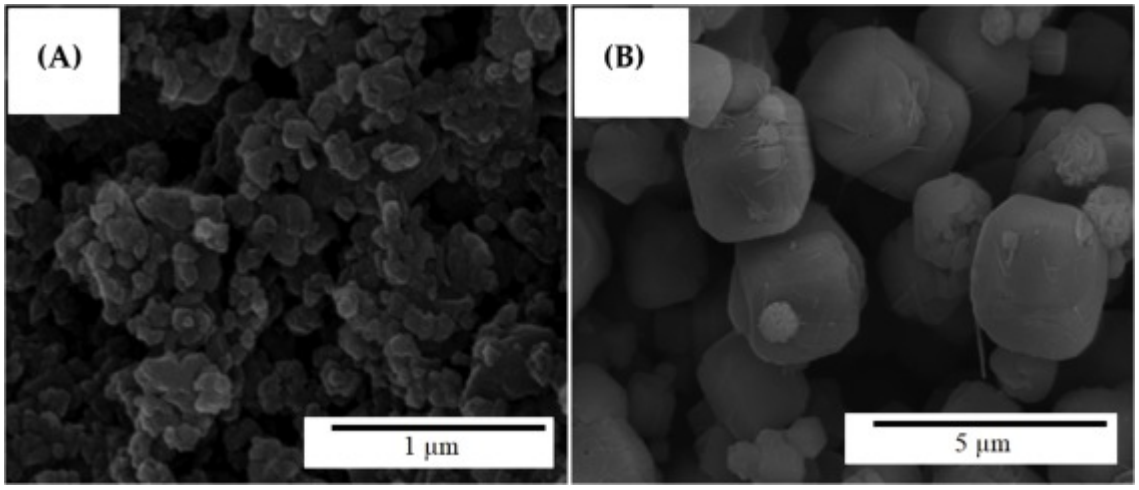

805 **Figure 1.** Scanning electron microscopy (SEM) micrographs of the as-received powders of: (**A**)

806 Silica (SiO_2) and (**B**) zeolite microparticles. Scale markers of 1 µm and 5 µm, respectively.

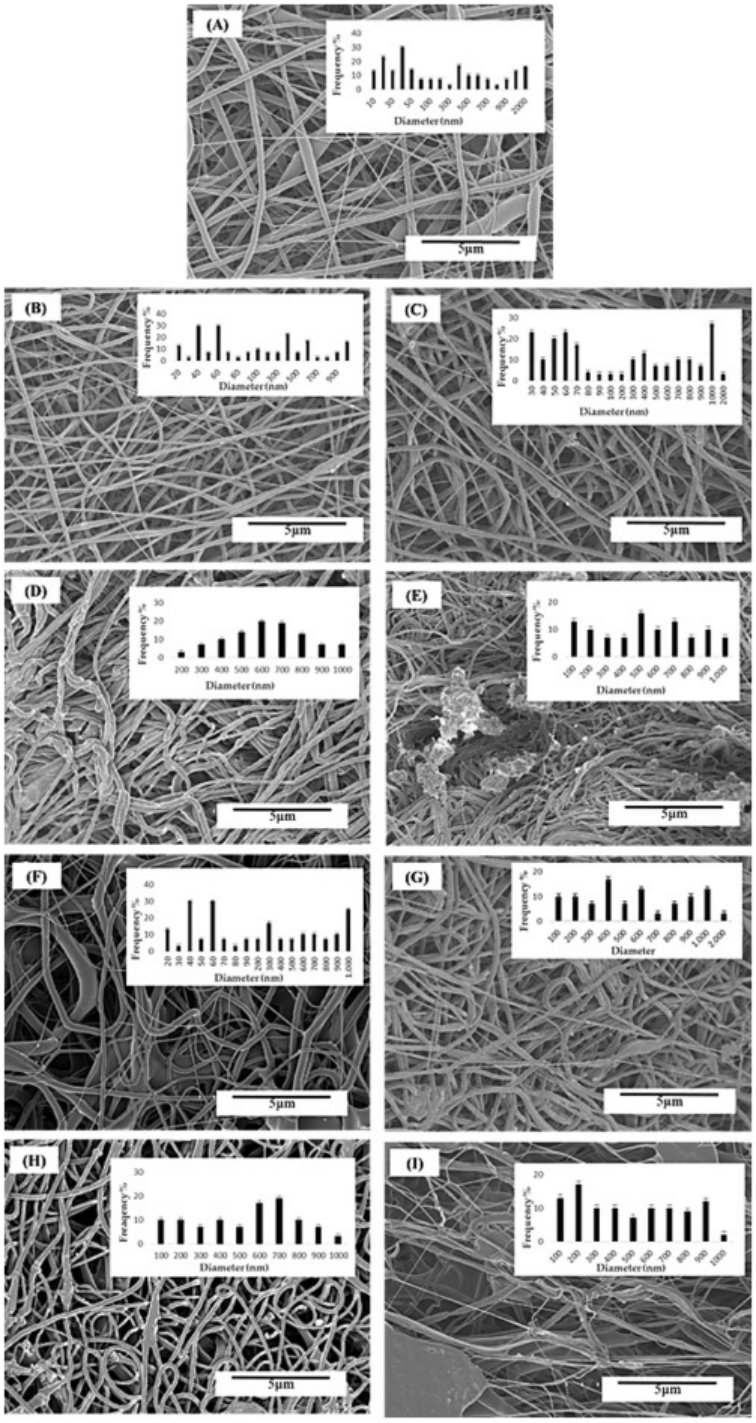

807

808 **Figure 2.** Scanning electron microscopy (SEM) micrographs of the electrospun fibers of: (**A**) Neat

809 poly(ε-caprolactone) (PCL); (**B**) PCL/silica (SiO_2) 5 wt%; (**C**) PCL/SiO_2 10 wt%; (**D**) PCL/SiO_2 15

810 wt%; (**E**) PCL/SiO_2 20 wt%; (**F**) PCL/zeolite 5 wt%; (**G**) PCL/zeolite 10 wt%; (**H**) PCL/zeolite 15

811 wt%; (**I**) PCL/zeolite 20 wt%. Fiber diameter histograms are in the insets and scale markers of 5 μm.

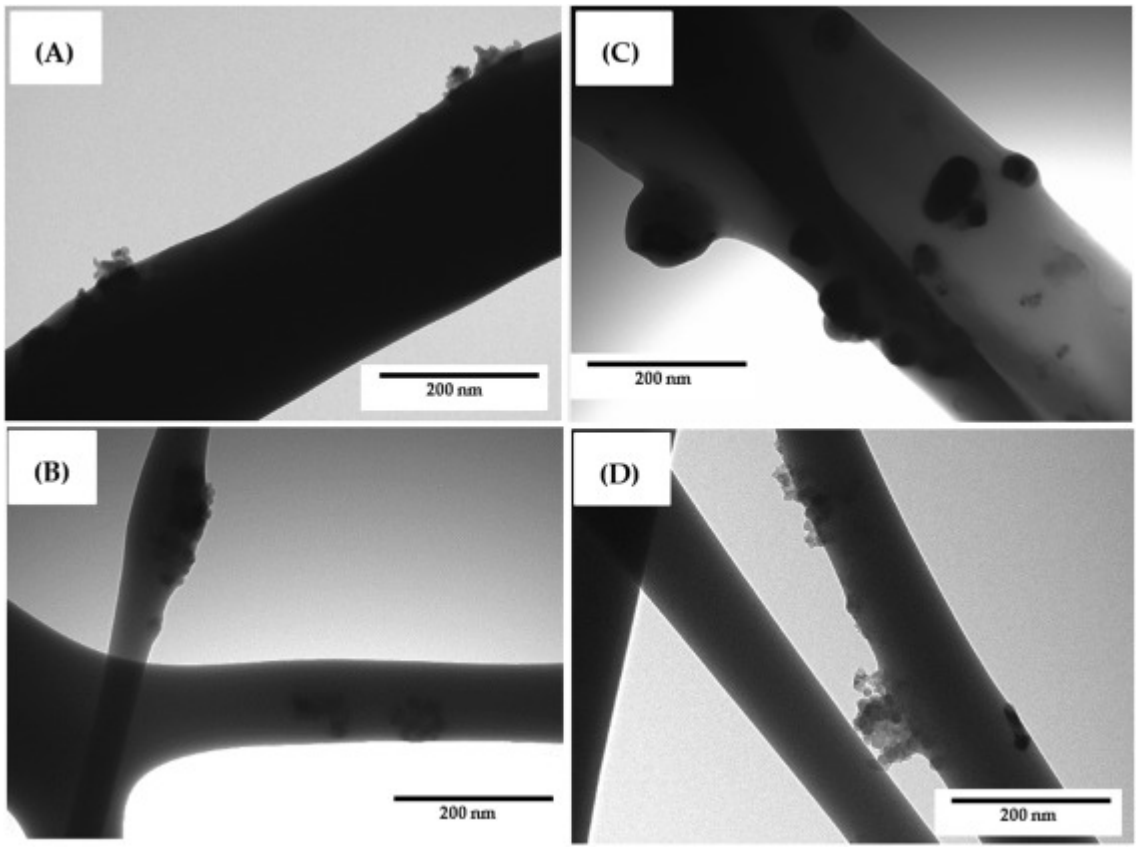

Figure 3. Selected transmission electron microscopy (TEM) micrographs of the electrospun fibers of: (**A**) Poly(ε-caprolactone) (PCL)/silica (SiO_2) 10 wt%; (**B**) PCL/SiO_2 20 wt%; (**C**) PCL/zeolite 10 wt%; (**D**) PCL/zeolite 20 wt%. Scale markers of 200 nm.

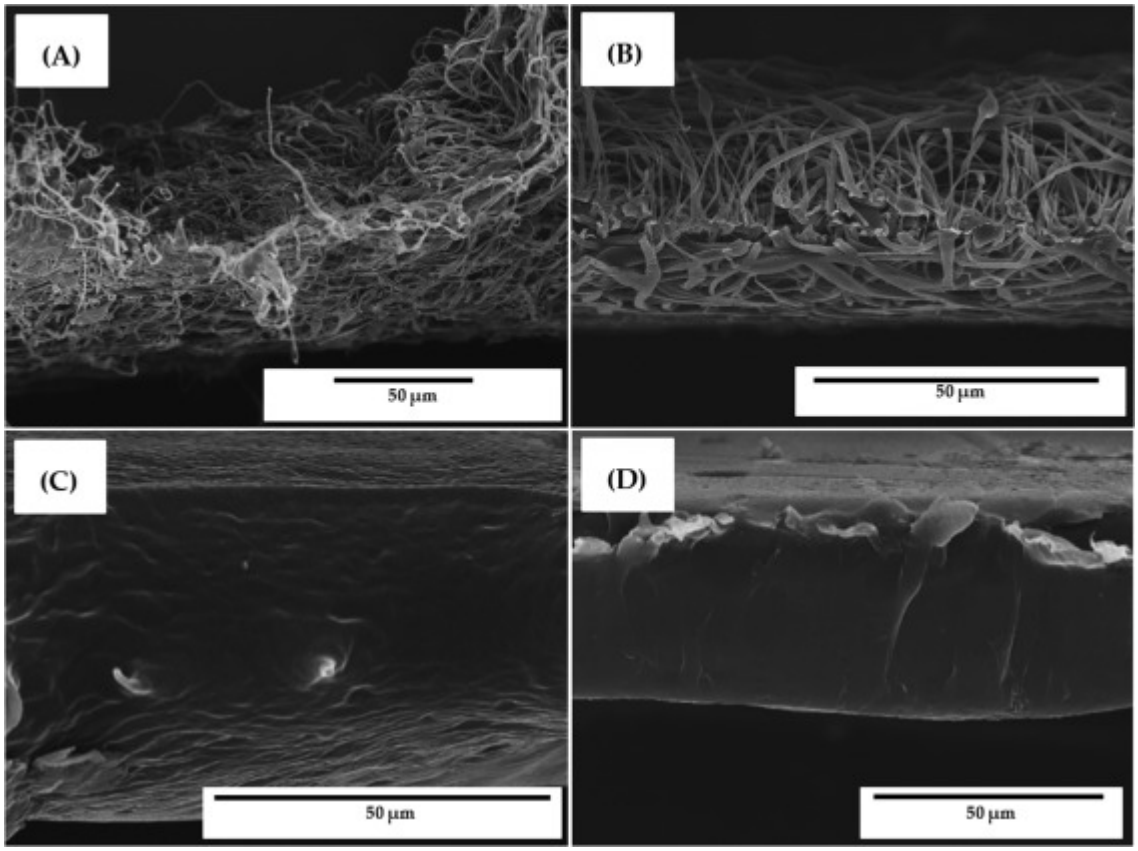

Figure 4. Scanning electron microscopy (SEM) micrographs of the electrospun mats of poly(ε-caprolactone) (PCL) thermally post-processed for 40 s, without pressure, at different temperatures: (**A**) No treatment; (**B**) 45 ºC; (**C**) 55 ºC; (**D**) 65 ºC. Scale markers of 50 µm.

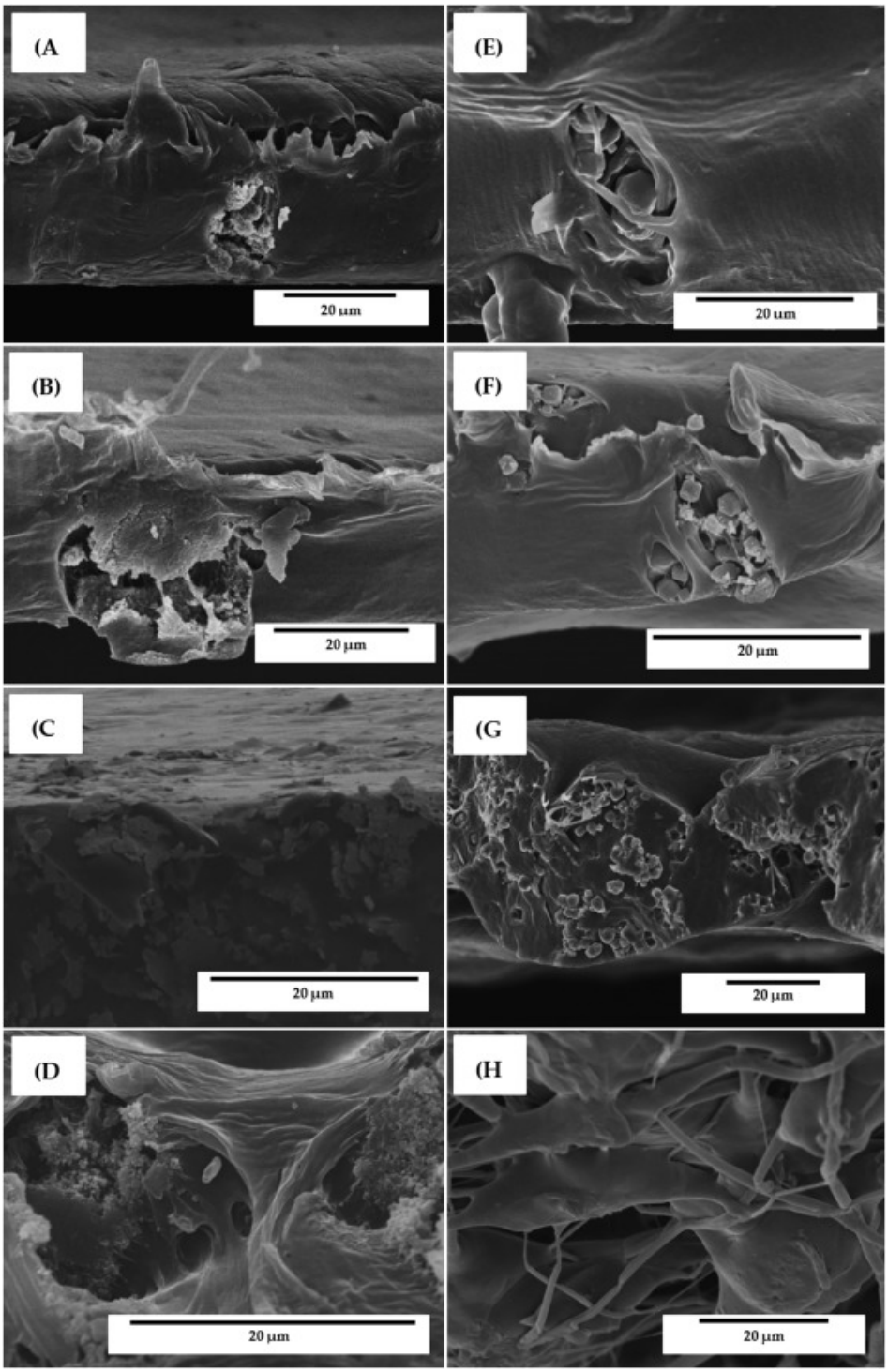

Figure 5. Scanning electron microscopy (SEM) micrographs of the electrospun mats thermally post-processed at 55 ºC for 40 s, without pressure, of: (**A**) Poly(ε-caprolactone) (PCL)/silica (SiO_2) 5 wt%; (**B**) PCL/SiO_2 10 wt%; (**C**) PCL/SiO_2 15 wt%; (**D**) PCL/SiO_2 20 wt%; (**E**) PCL/zeolite 5 wt%; (**F**) PCL/zeolite 10 wt%; (**G**) PCL/zeolite 15 wt%; (**H**) PCL/zeolite 20 wt%. Scale markers of 20 µm.

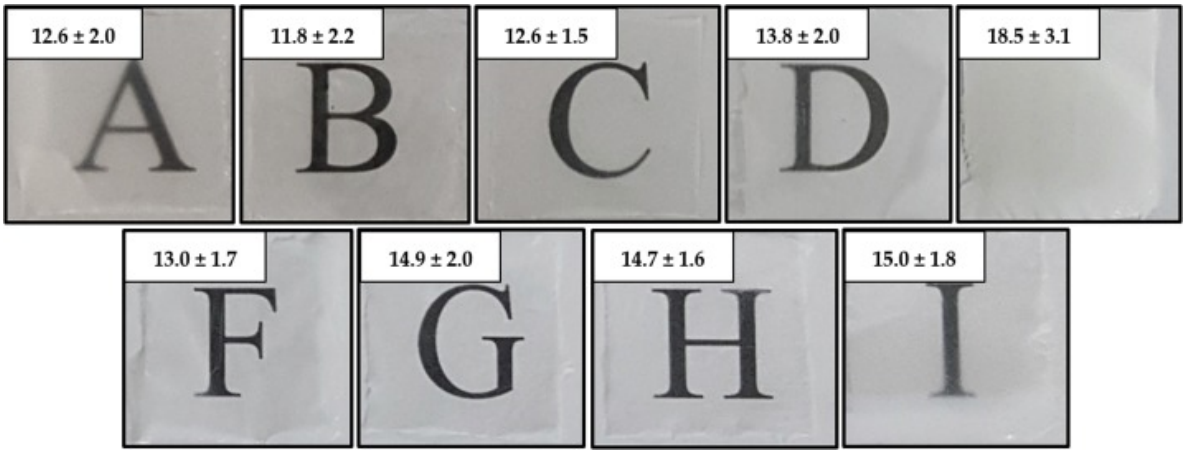

Figure 6. Visual appearance and contact transparency of the electrospun films of: (A) Poly(ε-caprolactone) (PCL); (B) PCL/zeolite 5 wt%; (C) PCL/zeolite 10 wt%; (D) PCL/zeolite 15 wt%; (E) PCL/zeolite 20 wt%; (E); PCL/silica (SiO_2) 5 wt% (F) PCL/ SiO_2 10 wt%; (G) PCL/SiO_2 15 wt%; (H) PCL/ SiO_2 20 wt%. Transparency (*T*) values are shown in the insets.

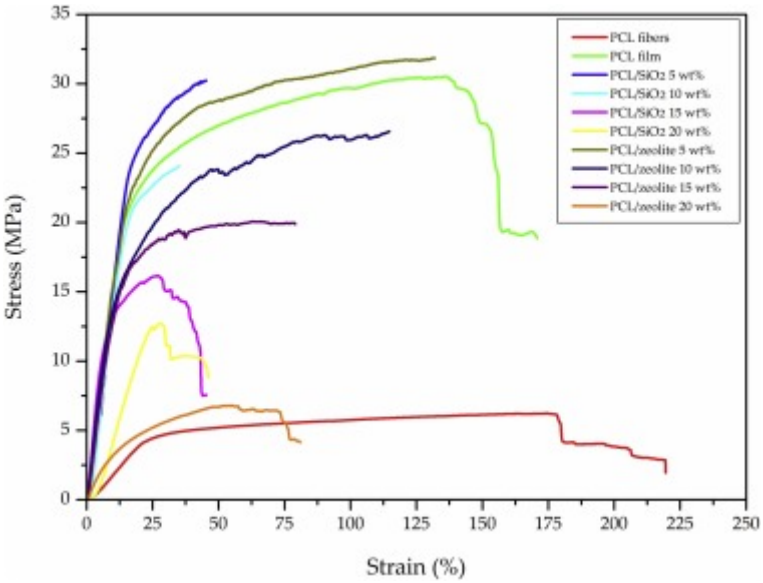

836

837 **Figure 7.** Tensile stress–strain curves of the electrospun fibers mat and films of poly(ε-caprolactone)

838 (PCL) containing zeolite and silica (SiO_2) microparticles.

Tables

Table 1. Values of viscosity, surface tension, and conductivity of the suspensions of poly(ε-caprolactone) (PCL) containing zeolite and silica (SiO_2) microparticles.

Suspension	Viscosity (Pa.s)	Surface Tension (mN/m)	Conductivity (µS/cm)
PCL	0.7548 ± 0.0526^{a}	27.8 ± 0.1^{a}	0.02 ± 0.01^{a}
PCL/SiO_2 5 wt%	0.9753 ± 0.0331^{b}	27.7 ± 0.1^{a}	0.10 ± 0.03^{b}
PCL/ SiO_2 10 wt%	1.1590 ± 0.0672^{c}	31.3 ± 0.2^{b}	0.07 ± 0.03^{c}
PCL/ SiO_2 15 wt%	1.5884 ± 0.0632^{d}	31.5 ± 0.2^{b}	0.11 ± 0.05^{b}
PCL/ SiO_2 20 wt%	1.8647 ± 0.0651^{e}	33.9 ± 0.3^{c}	0.19 ± 0.02^{b}
PCL/zeolite 5 wt%	0.7578 ± 0.0558^{a}	27.9 ± 0.1^{a}	0.02 ± 0.01^{a}
PCL/zeolite 10 wt%	1.0110 ± 0.0487^{c}	24.2 ± 0.2^{d}	0.01 ± 0.01^{d}
PCL/zeolite 15 wt%	2.2771 ± 0.0621^{f}	24.0 ± 0.2^{d}	0.02 ± 0.01^{a}
PCL/zeolite 20 wt%	8.1942 ± 0.0552^{g}	24.0 ± 0.2^{d}	0.01 ± 0.01^{d}

[a–g] Different letters in the same column indicate a significant difference among the samples ($p < 0.05$).

850 **Table 2.** Mechanical properties of the electrospun fibers mat and films of poly(ε-caprolactone) (PCL)
851 containing zeolite and silica (SiO_2) microparticles in terms of: tensile modulus (*E*), tensile strength
852 at yield (σ_y), elongation at break (ε_b).

Sample	E (MPa)	σ_y (MPa)	ε_b (%)
PCL fibers	19.6 ± 6.1 [a]	4.5 ± 0.8 [a]	183.9 ± 9.8 [a]
PCL film	188.3 ± 10.1 [b]	22.5 ± 3.4 [b]	162.5 ± 8.1 [b]
PCL/SiO_2 5 wt%	205.6 ± 13.0 [b]	26.4 ± 2.1 [b]	77.8 ± 5.1 [c]
PCL/ SiO_2 10 wt%	198.4 ± 12.0 [b]	21.6 ± 3.2 [b]	47.7 ± 5.2 [d]
PCL/ SiO_2 15 wt%	196.5 ± 10.1 [b]	16.0 ± 2.7 [c]	35.4 ± 7.3 [e]
PCL/ SiO_2 20 wt%	56.4 ± 9.9 [c]	12.9 ± 2.6 [d]	31.7 ± 6.9 [e]
PCL/zeolite 5 wt%	193.3 ± 12.0 [b]	27.3 ± 1.7 [b]	155.6 ± 20.0 [b]
PCL/zeolite 10 wt%	195.2 ± 21.0 [b]	22.1 ± 3.8 [b]	127.0 ± 14.4 [b]
PCL/zeolite 15 wt%	203.1 ± 17.0 [b]	19.1 ± 3.1 [bc]	84.6 ± 15.4 [c]
PCL/zeolite 20 wt%	63.8 ± 7.0 [c]	6.2 ± 2.1 [a]	68.0 ± 12.4 [c]

853 [a–e] Different letters in the same column indicate a significant difference among the samples ($p < 0.05$).

854 **Table 3.** Amount of histamine entrapped and binding capacity of the electrospun films of poly(ε-
855 caprolactone) (PCL) containing zeolite and silica (SiO_2) microparticles.

Samples	*Staphylococcus aureus*				*Salmonella* Paratyphi A			
	Histamine (mg/L)*	**Binding capacity (%)**	**pH****	**Bacterial growth (CFU/mL)*****	**Histamine (mg/L)**	**Binding capacity (%)**	**pH****	**Bacterial growth (CFU/mL)*****
Control*	0.721 ± 0.051	---	5.53± 0.01	14.04×10^7	0.771 ± 0.023	---	5.99± 0.02	16.32×10^7
PCL	0.039 ± 0.003 [a]	5.5 ± 0.1 [a]	5.67± 0.01	14.2×10^7	0.034 ± 0.007 [a]	4.4 ± 0.1 [a]	5.91± 0.01	16×10^7
PCL/SiO_2 5 wt%	0.434 ± 0.034 [b]	60.2 ± 0.8 [b]	5.51± 0.01	16.56×10^7	0.348 ± 0.016 [b]	45.1 ± 0.3 [b]	5.88± 0.02	15.02×10^7
PCL/ SiO_2 10 wt%	0.448 ± 0.037 [b]	62.1 ± 0.5 [b]	5.51± 0.01	16.12×10^7	0.392 ± 0.020 [c]	50.8 ± 0.6 [c]	5.91± 0.01	16.57×10^7
PCL/ SiO_2 15 wt%	0.530 ± 0.032 [c]	73.5 ± 0.3 [c]	5.55± 0.01	16.29×10^7	0.395 ± 0.031 [c]	51.2 ± 0.4 [c]	5.83± 0.01	17×10^7
PCL/ SiO_2 20 wt%	0.570 ± 0.021 [d]	79.1 ± 0.4 [d]	5.68± 0.02	14×10^7	0.428 ± 0.018 [d]	55.5 ± 1.1 [d]	5.9± 0.01	15.41×10^7
PCL/zeolite 5 wt%	0.592 ± 0.037 [d]	82.1 ± 1.2 [d]	5.66± 0.02	14.74×10^7	0.430 ± 0.025 [d]	55.8 ± 1.4 [d]	6.01± 0.02	16.71×10^7
PCL/zeolite 10 wt%	0.608 ± 0.017 [de]	84.3 ± 2.0 [de]	5.51± 0.01	14.58×10^7	0.453 ± 0.039 [de]	58.8 ± 2.3 [de]	5.96± 0.01	16.21×10^7
PCL/zeolite 15 wt%	0.622 ± 0.028 [de]	86.3 ± 1.9 [de]	5.51± 0.01	15.48×10^7	0.482 ± 0.142 [e]	62.5 ± 3.2 [e]	5.89± 0.01	16.43×10^7
PCL/zeolite 20 wt%	0.650 ± 0.031 [e]	90.2 ± 3.2 [e]	5.61± 0.02	15.02×10^7	0.614 ± 0.232 [f]	79.6 ± 4.0 [f]	5.99± 0.03	16.23×10^7

856 * Histamine production capacity for each bacterium after 72 h

857 **pH of each solution after 72 h (Initial pH was adjusted to 6 for each solution.)

858 ***Bacterial growth after 72 h (The initial bacterial count for *S. aureus* and *S.* Paratyphi A were 1.45×10^7 and 1.3×10^7 CFU/ml
859 respectively.)

860 [a–f] Different letters in the same column indicate a significant difference among the samples ($p < 0.05$).

861